

# Understanding the reaction mechanism of Kolbe electrolysis on Pt anodes

Sihang Liu<sup>1#</sup>, Nitish Govindarajan<sup>1#</sup>, Hector Prats<sup>1,2</sup>, Karen Chan<sup>1\*</sup>

1. Catalysis Theory Center, Department of Physics, Technical University of Denmark (DTU), 2800 Kgs. Lyngby, Denmark

2. Department of Chemical Engineering, University College London, Roberts Building, Torrington Place, London WC1E 7JE, UK

\*Corresponding author: Email: [kchan@fysik.dtu.dk](mailto:kchan@fysik.dtu.dk)

\*Lead contact: Email: [kchan@fysik.dtu.dk](mailto:kchan@fysik.dtu.dk)

#These authors contributed equally

## SUMMARY

Kolbe electrolysis has been proposed as an efficient electrooxidation process to synthesize (un)symmetrical dimers from biomass-based carboxylic acids. However, the reaction mechanism of Kolbe electrolysis remains controversial. In this work, we develop a density functional theory based microkinetic model to study the reaction mechanism of Kolbe electrolysis of acetic acid ( $\text{CH}_3\text{COOH}$ ) on both pristine and partially oxidized Pt anodes. We show that the shift in the rate-determining step of oxygen evolution reaction (OER) on  $\text{Pt}(111)@\alpha\text{-PtO}_2$  surface from  $\text{OH}^*$  formation to  $\text{H}_2\text{O}$  adsorption gives rise to the large Tafel slopes, i.e., the inflection zones, observed at high anodic potentials in experiments on Pt anodes. The activity passivation as a result of the inflection zone is

further exacerbated in the presence of Kolbe species (i.e.,  $\text{CH}_3\text{COO}^*$  and  $\text{CH}_3^*$ ). Our simulations find the  $\text{CH}_3\text{COO}^*$  decarboxylation and  $\text{CH}_3^*$  dimerization steps determine the activity of Kolbe reaction during inflection zone. In contrast to the  $\text{Pt}(111)@ \alpha\text{-PtO}_2$  surface,  $\text{Pt}(111)$  shows no activity towards Kolbe products as the  $\text{CH}_3\text{COO}^*$  decarboxylation step is limiting throughout the considered potential range. This work resolves major controversies in the mechanistic analyses of Kolbe electrolysis on Pt anodes: the origin of the inflection zone, and the identity of the rate limiting step.

## INTRODUCTION

With the electrochemical conversion of biomass derivatives as a potential means of green chemical production<sup>1-3</sup>, electro-organic synthesis is experiencing a revival<sup>4-10</sup>. Compared to conventional catalytic (de)-hydrogenation reactions, electrocatalytic conversion schemes offer several advantages: a) they operate at ambient conditions, b) they can be powered by sustainable electricity from wind and solar energy, and c) they require only water as the proton source instead of expensive hydrogen feeds<sup>11-13</sup>. Kolbe electrolysis is a central reaction in electro-organic synthesis since it could be applied to produce functionalized homo/hetero-dimers with high selectivity<sup>14-16</sup> and even the same chirality<sup>17</sup>. Currently, the feedstock for Kolbe electrolysis, i.e., carboxylic acids, could be derived from biomass resources<sup>18</sup>, which further increases the sustainability of this reaction. The electrolysis of carboxylic acid was first observed by Faraday<sup>19</sup>, and Hermann Kolbe identified ethane and octane as the respective products of the electrolysis of acetic and valeric acid<sup>20</sup>. In the past century, a number of experimental studies have investigated its mechanism and the impact of reaction conditions on activity<sup>21-25</sup>.

**Scheme 1(a)** shows the main mechanisms proposed for (non)-Kolbe electrolysis reactions.<sup>14,16</sup> Carboxylic acids (R-COOH) undergo a proton-coupled electron transfer (PCET) to form adsorbed carboxyl species (R-COO\*). Following decarboxylation of R-COO\* which produces CO<sub>2</sub> as a by-product, the resultant R\* either dimerizes to form prolonged alkanes (R-R, Kolbe reaction, denoted in black) undergoes disproportionation, or loses a further electron to form a R<sup>+</sup> carbocation species (non-Kolbe reactions, denoted in grey). This R<sup>+</sup> species can undergo a further H<sup>+</sup> loss to form alkenes (R<sub>2</sub>), hydrolysis to form alcohols (R-OH), or react with the deprotonated carboxylic acid (R-COO<sup>-</sup>) to produce esters. The oxygen evolution reaction (OER, not shown) is the major side reaction that occurs during Kolbe electrolysis at the anode under aqueous conditions, while it is suppressed under anhydrous conditions.<sup>21,26</sup> Pt (in oxidized form under operating conditions) is the most widely studied anode for Kolbe electrolysis, and other noble metal oxides like IrO<sub>2</sub>, RuO<sub>2</sub>, and graphene have also been shown to be active for this reaction<sup>16,18,25-27</sup>.

The electro-oxidative conversion of acetic acid to ethane on Pt anodes is the simplest of all Kolbe reactions (**Scheme 1b**). A prominent feature for this particular process is a flat 'inflection zone' in the current-potential curves (see Figure 3a, below), which coincides with a transition between the predominance of O<sub>2</sub> production via OER at lower potentials to ethane production (Kolbe reaction) at higher potentials<sup>30-32</sup>. Kolbe electrolysis of other carboxylic acids on Pt and Ir also show inflection zones at high potentials that accompany the selectivity transition from OER to the Kolbe reaction<sup>33-35</sup>.

In the earliest mechanistic studies, Crum-Brown, Walker and co-workers proposed that Kolbe reaction is a free radical reaction (i.e., homogeneous solution phase reaction),

which does not directly involve the electrode surface<sup>36–38</sup>. This free-radical theory was later refuted by rotating electrode<sup>35</sup> and pulsed electrolysis<sup>39</sup> experiments on Pt anodes, which showed that the electrode surface promotes the reaction rate and that Kolbe species reversibly adsorb on the Pt electrode.

Despite the decades of exploration of Kolbe electrolysis, there remain several open questions regarding the exact details of its surface-catalyzed mechanism: i) The possible rate-determining steps (RDS) throughout the operating potentials, ii) The mechanistic origin of the inflection zone on Pt and Ir anodes observed in experiments, and iii) The relationship between Kolbe and OER in aqueous solutions.

All three elementary steps in the surface-catalyzed process in **Scheme 1b** have been proposed to be the rate determining step (RDS)<sup>21</sup>. If the first and only electron transfer step, the discharge and deprotonation of  $\text{CH}_3\text{COOH}$ <sup>40</sup>, were rate limiting, there would be very low coverages of  $\text{CH}_3\text{COO}^*$  and  $\text{CH}_3^*$  species. However, it was reported by transient studies that ethane only starts being produced under high potentials where there are high surface coverages of Kolbe species<sup>41–43</sup>. This build-up of evident coverages of Kolbe species excludes the discharge of  $\text{CH}_3\text{COOH}$  to  $\text{CH}_3\text{COO}^*$  from being the RDS, such that only the later decarboxylation and/or coupling steps can be rate limiting.

Two theories have been postulated for the presence of the inflection zone observed during the electrolysis of acetic acid on Pt anodes:

*Theory I:* Cervino et al. suggested that this inflection zone arises from changes in the coverage of the surface species from  $\text{CH}_3\text{COO}^*$  species below the inflection zone to further Kolbe intermediates, probably  $\text{CH}_3^*$ , above the inflection zone<sup>41</sup>. They made this postulation based on their observation of a shift in the electrode capacitance at potentials

within the inflection zone, determined using electrochemical impedance spectroscopy. This shift in  $\text{CH}_3^*$  coverage was also observed in a voltammetric study by Vasini et al<sup>42</sup>. *Theory II*: Conway and Dzieciuch<sup>22,44,45</sup> attributed the inflection zone to a selectivity transition from  $\text{O}_2$  to ethane. They postulate that this transition occurs upon sufficient build-up of a “barrier-layer” film of  $\text{CH}_3\text{COO}^*$  at high enough potentials where  $\text{CH}_3\text{COOH}$  is favored. The build-up of such a “barrier layer” would hinder the adsorption of  $\text{H}_2\text{O}$  or  $\text{OH}^-$  species (the reactants of OER) on the surface and thereby suppress OER<sup>35</sup>. Consistent with this theory, such a film is absent on gold and nickel, which are inactive catalysts for Kolbe electrolysis. However, since there is limited amount of data for the partial (vs. total) current densities towards the various products, it is not clear that OER is suppressed upon the build-up of such a film.

The large Tafel slopes ( $> 120$  mV/dec) of the total current densities in experiments of Kolbe electrolysis was also suggested to arise from the presence of the barrier-layer film of *Theory I*<sup>1</sup>. This theory attributes such large Tafel slopes and correspondingly small effective symmetry factors ( $\beta \ll 0.5$ ) to the reduction in the metal-solution potential drop in the presence of a barrier film of Kolbe species. Moreover, OER on pre-oxidized Pt anodes also shows extremely large Tafel slopes ( $> 500$  mV/dec) at high potentials, indicating a barrier-layer of Kolbe species is not necessarily the decisive factor for the large Tafel slopes at high potentials in electrolysis<sup>46</sup>.

As for the nature of electrode surface, Pt should be oxidized under the typical operating conditions ( $> 1.5$  V vs. RHE) for Kolbe electrolysis, with the formation of several stable oxide overlayers<sup>43,47,48</sup>. In a previous study, Koper et al. showed that  $\alpha\text{-PtO}_2$  layer are generated at ca. 1 V vs. RHE on smooth Pt(111) single crystals in aqueous solution via

*in situ* vibrational spectroscopy<sup>49</sup>. These observations are consistent with density functional theory (DFT) calculations<sup>50,51</sup> which suggest the formation of  $\alpha$ -PtO<sub>2</sub> on smooth Pt anodes to be thermodynamically favored above ca. 1 V vs. RHE. (cf. the Pourbaix diagram in **Figure S1**).

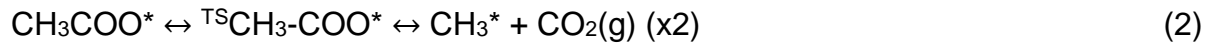
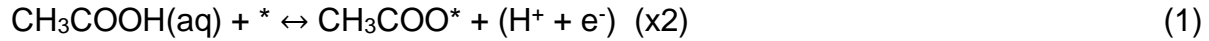
In this work, we present a theory-based understanding of mechanisms for Kolbe electrolysis of acetic acid on Pt anodes. Based on DFT calculations of reaction energetics, we find that the strong binding configuration of CH<sub>3</sub>COO\* on Pt(111) at low potentials severely impedes the subsequent decarboxylation steps on this surface, while its weakened in-plane adsorption on the Pt(111)@ $\alpha$ -PtO<sub>2</sub> surface at more oxidizing potentials results in facile C-C bond breaking and the subsequent CH<sub>3</sub>\* coupling step towards the formation of ethane. Combining microkinetic simulations and previously reported experimental studies, we show that the inflection zone observed in Kolbe electrolysis at high anodic potentials arises from a levelling off in OER activity on the oxidized Pt surface. The degree of rate control (DRC) analysis indicates the total activity passivation observed during the inflection zone results from a shift in RDS for the OER from OH\* formation to H<sub>2</sub>O adsorption that is further exacerbated by the presence of Kolbe species. The DRC analysis also shows that later chemical steps (the decarboxylation and C-C coupling steps) are rate-determining in the formation of ethane. Finally, we compare and contrast the findings of the present vs. previous mechanistic studies.

## RESULTS

In what follows, we present the elementary steps and reaction energetics for Kolbe electrolysis of acetic acid and OER on Pt(111) and Pt(111)@ $\alpha$ -PtO<sub>2</sub> model surfaces, followed by microkinetic simulations to estimate the activity and selectivity towards the various products.

We considered the following elementary steps for Kolbe electrolysis and the competing OER reaction, as suggested by previous studies<sup>15,21,52,53</sup>:

Kolbe reaction:



Oxygen evolution reaction (OER):



where \* denotes the surface sites for adsorption. In addition to the thermodynamics of the elementary steps, we have computed explicitly  ${}^{\text{TS}}\text{CH}_3\text{-COO}^*$  and  ${}^{\text{TS}}\text{CH}_3\text{-CH}_3^*$ , the transition states corresponding to the decarboxylation of  $\text{CH}_3\text{COO}^*$  and dimerization of  $\text{CH}_3^*$  respectively, which interact significantly with the interfacial electric field and are decisive in the reaction energetics, as we discuss below. We have, for simplicity, neglected non-Kolbe processes in this analysis.

## **Adsorption strength of reaction intermediates is tuned by the interfacial electric field**

Like in e.g., the oxygen reduction reaction<sup>54</sup> and CO<sub>2</sub> reduction reaction<sup>55–58</sup>, we found adsorbate-field interactions to significantly affect the reaction energetics for both Kolbe electrolysis and the competing OER. **Figure 1** shows the computed effects of the electric field ( $\vec{E}$ ) for the adsorption energies of the reaction intermediates and transition state energies from Eqs. (1-8) on both the investigated surfaces. The corresponding  $V_{\text{SHE}}$  is estimated based on the Helmholtz capacitance ( $C_{\text{H}}$ ) and potential of zero charge ( $U_{\text{PZC}}$ ) for Pt (111) and Pt(111) $\alpha$ -PtO<sub>2</sub>, obtained from Ref<sup>59</sup>.

At ca. 1.0 V/Å, there are significant field stabilizations ( $\sim 0.1 - 1\text{V}$ ) of both OER and Kolbe reaction intermediates. Amongst the OER intermediates, we find OOH\* to have the largest stabilizing effect at higher potentials due to its comparatively large polarizability ( $\alpha$ )<sup>54</sup>. With the exception of OOH\*, the field effects on the Kolbe intermediates are generally larger than those for OER. As we discuss below, the field-adsorbate interactions for both the C-C bond breaking (Eq. 2) and CH<sub>3</sub> dimerization (Eq. 3) steps have an important influence on the energetics of the Kolbe reaction on both surfaces considered.

## **Free energy diagrams indicate facile Kolbe activity on oxidized metal surfaces at high potentials**

**Figures 2** shows the calculated free energy profiles for Kolbe electrolysis of acetic acid and the competing OER reaction on Pt(111) and Pt(111) $\alpha$ -PtO<sub>2</sub>, respectively. We include the elementary steps of Eqs (1-8) at potentials of 1, and 2 $V_{\text{SHE}}$  under reaction



conditions of  $\text{pH} = 4.6$ ,  $C_a$  (initial concentration of acetic acid) = 1M,  $T = 298$  K. The field effects, shown in **Figure 1**, are also included. In the Kolbe reaction, only the initial deprotonation steps (which occurs twice in the overall reaction) are electrochemical (i.e., involve a proton-coupled electron transfer), while the subsequent decarboxylation and dimerization steps are chemical. For comparison, the free energy diagrams without adsorbate-field interactions are shown in **Figure S6**. Note that no solvation corrections were applied here, because we assume that the effect of solvation on activity is minor compared to the effect of large potential change (1.5 V vs RHE) considered in our calculations.

In general,  $\text{Pt}(111)@ \alpha\text{-PtO}_2$  binds both Kolbe and OER species more weakly than  $\text{Pt}(111)$ . Specifically,  $\text{CH}_3\text{COOH}$  deprotonation is much more sluggish on  $\text{Pt}(111)@ \alpha\text{-PtO}_2$  than  $\text{Pt}(111)$  at 1  $V_{\text{SHE}}$  in **Figure 2a** and **2b**, indicating a high overpotential for building up  $\text{CH}_3\text{COO}^*$  species on Pt oxides. Consequently, OER species should dominate on  $\text{Pt}(111)@ \alpha\text{-PtO}_2$  at low potentials, while  $\text{CH}_3\text{COO}^*$  could already build up on  $\text{Pt}(111)$ .

At higher potentials, the adsorption of  $\text{CH}_3\text{COO}^*$  becomes facile on both surfaces. The defining differences between the two surfaces is in the adsorption configuration of  $\text{CH}_3\text{COO}^*$  and the magnitude of the subsequent C-C bond breaking barrier. These differences result in surmountable barriers for the Kolbe reaction on  $\text{Pt}(111)@ \alpha\text{-PtO}_2$  but not on  $\text{Pt}(111)$ . **Figures 2c** and **2d** show side and top views of  $\text{CH}_3\text{COO}^*$  on the two respective surfaces. On  $\text{Pt}(111)$ ,  $\text{CH}_3\text{COO}^*$  is adsorbed in a stable bidentate configuration, which has been confirmed by attenuated total reflection configuration (ATR-FTIRS) studies<sup>60</sup>. The corresponding free energy for the proton-electron transfer step (Eq. 1) is exergonic, even at 0  $V_{\text{SHE}}$ , well below the oxidizing potentials at which Kolbe

electrolysis occurs. In contrast,  $\text{CH}_3\text{COO}^*$  is weakly adsorbed in-plane on  $\alpha\text{-PtO}_2$  with a flexible configuration for further reactions, due to the presence of surface O atoms and the longer Pt-Pt distance of ca. 3.2 Å relative to ca. 2.8 Å on Pt(111) model. The free energy for the proton-electron transfer step (Eq. 1) becomes exergonic only at 1.33  $V_{\text{SHE}}$ . The subsequent C-C bond breaking (the decarboxylation step, Eq. 2), on the other hand, is much more facile for the  $\text{CH}_3\text{COO}^*$  on  $\alpha\text{-PtO}_2$  than Pt(111). As illustrated in **Figure 2c**, there is a large configurational energy penalty for the rotation required to break the C-C bond on the Pt(111) surface. In contrast, the in-plane configuration of  $\text{CH}_3\text{COO}^*$  on  $\alpha\text{-PtO}_2$  (cf. Figure 2d) enables a pseudo-homogeneous path for C-C bond breaking that is much more facile.

Both chemical steps exhibit potential dependence to some extent due to adsorbate dipole-field interactions (**Figures 1a, b**). These interactions result in a reduction in the barrier of C-C bond breaking from 2.07 eV to 1.55 eV on Pt(111) and a slight increase from 0.20 to 0.23 eV on Pt(111) $\text{@}\alpha\text{-PtO}_2$  when the potential increases from 1V to 2 $V_{\text{SHE}}$  in (**Figures 2a, b**). Despite the field stabilization, the C-C bond breaking barrier on Pt(111) is still too large for any activity towards the Kolbe reaction at ca. 2  $V_{\text{SHE}}$ .

The subsequent  $\text{CH}_3\text{-CH}_3$  dimerization barrier (Eq. 3) is also field-stabilized on both surfaces. The calculated barriers change from 1.31 to 1.29 eV on Pt(111) and from 0.76 to 0.28 eV on Pt(111) $\text{@}\alpha\text{-PtO}_2$ ; the reduced barrier of  $\text{CH}_3^*$  dimerization on  $\alpha\text{-PtO}_2$  surface further facilitates ethane ( $\text{C}_2\text{H}_6$ ) formation.

In summary, the field-dependent reaction energetics predict that the Kolbe reaction proceeds on Pt(111) $\text{@}\alpha\text{-PtO}_2$  but not Pt(111) at high potentials (ca. 2  $V_{\text{SHE}}$ ). On Pt(111) $\text{@}\alpha\text{-PtO}_2$  at this potential range, there is a buildup of  $\text{CH}_3\text{COO}^*$  coverage, followed

by facile C-C bond breaking and CH<sub>3</sub>-CH<sub>3</sub> dimerization. In contrast, due to the high barriers for the C-C bond breaking of CH<sub>3</sub>COO\* on Pt(111), a coverage of CH<sub>3</sub>COO\* would simply build up and act as a surface poison.

### **Microkinetic modeling suggests Kolbe electrolysis to be limited by decarboxylation and/or dimerization**

Based on the field-dependent energetics illustrated above, we develop a mean-field microkinetic model to determine the theoretical activity and selectivity of Kolbe electrolysis, which we directly compare to the experimental observations.

The experimental polarization curves taken from Ref<sup>30</sup> are displayed in **Figure 3a**. Inflection zones, nearly flat regions in the plots, appear above 2.1 V<sub>SHE</sub>. The onset current density reduces with an increase in the initial concentration of acetic acid in the electrolyte. The selectivity shifts from OER (O<sub>2</sub> production) towards Kolbe reaction (CO<sub>2</sub> and C<sub>2</sub>H<sub>6</sub> production) within the inflection zone. Both the production of O<sub>2</sub> and C<sub>2</sub>H<sub>6</sub> grow with increasing potentials, but the increase in C<sub>2</sub>H<sub>6</sub> production is more acute than O<sub>2</sub> production, which gives rise to the selectivity shift. The total selectivity of OER and Kolbe reactions reported in the experiments is ca. 90%, which may be due to side (e.g., Non-Kolbe and electrode oxidation) reactions or because methane that can be formed as a minor product from CH<sub>3</sub>\* was not accounted for in the product analysis in Ref<sup>30</sup>.

The qualitative features in the simulated total  $j$  vs. V<sub>SHE</sub> on Pt(111)@α-PtO<sub>2</sub> (**Figure 3b**) are consistent with the experimental observations in terms of the presence of the “inflection zone” (region of passivated activity) in  $j^{\hat{1}}$ . The simulated partial current densities in **Figure 3C** show the inflection zone arises from the suppression of OER

activity, which occurs along with a steady increase in the activity for the Kolbe reaction at high potentials. The selectivity shift from OER to Kolbe reaction is shown in **Figure 3d**, where our simulated results agree well with the experiment. Within the potential range 1.5-2.5  $V_{\text{SHE}}$ , Kolbe species, i.e., first  $\text{CH}_3^*$  and later  $\text{CH}_3\text{COO}^*$ , dominate on the surface, while OER species, e.g.,  $\text{H}_2\text{O}^*$ , peaks at ca. 2  $V_{\text{SHE}}$  and then decreases, shown in **Figure 3e**.

The DRC in **Figure 3f** also suggests that in the inflection zone, Kolbe reaction is limited by the barrier for  $\text{CH}_3^*$  coupling ( $^{\text{TS}}\text{CH}_3\text{-CH}_3^*$ ) as well as the coverage of preceding species as determined by  $^{\text{TS}}\text{CH}_3\text{-COO}^*$ . The small simulated Tafel slope ( $< 59\text{mV/dec}$ ) is consistent with a rate-limiting step after the first PCET step. Considering the intrinsic error in DFT calculations (ca. 0.2 eV), we suggest that the Kolbe reaction can be determined by decarboxylation and/or dimerization step at high potentials.

We directly compare the partial activities towards OER and Kolbe products between theory and experiment in **Figure 4**. The large Tafel slope of 528 mV/dec simulated for OER during inflection zone is comparable to that in experiments. The calculated Tafel slopes for Kolbe reaction is 47 mV/dec, in good agreement with experimental values ca. 56-66 mV/dec in Ref<sup>30,41</sup>, indicating it is not the  $\text{CH}_3\text{COO}^*$  formation (i.e., the first electron transfer step) but a later step that is limiting, i.e., the decarboxylation of  $\text{CH}_3\text{COO}^*$  and/or dimerization of  $\text{CH}_3^*$ .

We note that our microkinetic model presents a negative one-third order dependence of activity on  $\text{CH}_3\text{COOH}$  concentration shown in **Figure S7**, while the experimental dependence is almost negative first order (**Figure S8**). The degree of rate control (DRC) analysis in **Figure 3f** shows that OER activity (top panel) within inflection zone is

determined by  $\text{H}_2\text{O}^*$  adsorption and worsened by  $\text{CH}_3^*$  formation, which would in principle give rise to a negative first-order dependence on initial  $\text{CH}_3\text{COOH}$  concentration in solution. The discrepancy between the model and experiment could result from the sensitivity of adsorbate interaction parameters ( $\epsilon$ ) applied to account for adsorbate-adsorbate interactions in our model<sup>62,63</sup>. We show that applying a smaller adsorbate interaction factor for all species leads to ca. three-fourth order of dependence in **Figure S10**. Given the uncertainty in determining  $\epsilon$ , the negative dependence on reactant concentration still holds.

### **The low-overpotential part of the inflection zone arises from OER, and occurs even without acetic acid**

In order to deconvolute the effects of OER and Kolbe reaction, we explored OER in the absence of any Kolbe reaction (i.e.,  $C_a = 0$  M) on Pt oxide using microkinetic modeling. In **Figure S11a**, we show that without  $\text{CH}_3\text{COOH}$ , the simulated OER activity on  $\text{Pt}(111)@ \alpha\text{-PtO}_2$  is much higher than those with  $\text{CH}_3\text{COOH}$ . In **Figure S11b**, we further show that the coverages of OER species, are almost constant at high potentials, without the decrease that we observe in the presence of  $\text{CH}_3\text{COOH}$ . Interestingly, the OER also reaches inflection zone at higher potentials compared to the model with acetic acid. This is due to  $\text{H}_2\text{O}^*$  adsorption, i.e., a chemical step, is determining the OER activity at high potentials, where all PCET steps become facile. Our observations also indicate that reducing the partial pressure of water ( $p_{\text{H}_2\text{O}}$ ) in our microkinetic simulation lowers the OER activity within the inflection zone (cf. **Figure S12**). In the limit of anhydrous conditions ( $p_{\text{H}_2\text{O}} = 0$ ), there is no inflection zone, as there is no competition between OER with the

Kolbe reaction in this extreme case. This conclusion is also in line with previous observations that the Kolbe synthesis proceeds with optimal selectivity in nonaqueous media, e.g., in pure carboxylic acid solutions<sup>43,64</sup>, methanol<sup>65,66</sup> or other solvents<sup>16</sup>.

We note that the appearance of an inflection zone during OER has not been discussed in previous studies, probably due to the limited potential ranges (ca. 1.2- 2.0  $V_{\text{SHE}}$ ) typically investigated in previous studies. There is one study where the OER polarization curve on  $\text{PtO}_2$  films beyond 2  $V_{\text{SHE}}$  was reported where we observe the appearance of an inflection zone with a large Tafel slope ( $> 500$  mV/dec) (cf. **Figure S13**)<sup>46</sup>. It has been postulated that electron tunneling issues due to the formation of thick Pt oxide films might be the reason for the observed increase in Tafel slopes at high anodic potentials<sup>67-69</sup>. We anticipate that future studies can investigate the exact origin of the dramatic increase in Tafel slopes during OER.

In the context of the discussions on the inflection zone observed during OER discussed above, we emphasize the importance of accounting for  $\text{H}_2\text{O}$  binding as an explicit step in OER modeling studies, as this step is typically excluded based on the conventional assumption that  $\text{H}_2\text{O}$  adsorption is a facile chemical step<sup>70</sup>. However, the exclusion of  $\text{H}_2\text{O}$  adsorption in kinetic analysis could lead to following pitfalls: 1. For surfaces that bind  $\text{H}_2\text{O}$  strongly, such an exclusion could intrinsically underestimate the actual deprotonation barrier of  $\text{H}_2\text{O}^*$ ; 2. The competition for surface sites between  $\text{H}_2\text{O}$  and species for other reactions cannot be captured if the  $\text{H}_2\text{O}$  adsorption step is excluded in the modeling, e.g., like in  $\text{H}_2\text{O}^*$  vs  $\text{CH}_3\text{COO}^*$  in this work.

**Bare Pt(111) shows no activity for the Kolbe reaction in aqueous phase**

In contrast to Pt(111)@ $\alpha$ -PtO<sub>2</sub>, we find only OER occurs on Pt(111), while Kolbe reaction is prohibited by the high decarboxylation barrier shown in **Figure 2a**. The DRC analysis in **Figure S18** shows that Kolbe reaction is hindered by the formation of CH<sub>3</sub>-COO<sup>TS\*</sup>, and later also by the accumulation of CH<sub>3</sub>COO\*. As shown in **Figure S19**, the coverage of OER species decreases dramatically after ca. 1.1 V<sub>SHE</sub>, while CH<sub>3</sub>COO\* is swiftly building up. Finally, the consequent over-accumulation of CH<sub>3</sub>COO\* poisons the surface and leads to dramatic activity decline beyond 1.1 V<sub>SHE</sub> shown in **Figure S20**.

### **Sensitivity analysis of the microkinetic model**

To evaluate the generality of the conclusions of our microkinetic model, we perform sensitivity analyses on a few important model parameters as discussed below.

First, we note that only the reaction thermodynamics of the proton-electron transfers in Eqs 4-8 were considered for OER in our microkinetic model (i.e., these reactions are assumed to have negligible barriers)<sup>53,71</sup>, which might result in an overestimation of the OER activity on both surfaces considered. In **Figure S14** we show a sensitivity analysis of the barrier for O\* to OOH\*, which has been shown to be potentially determining PCET step in ORR on oxide surfaces<sup>53</sup>. With additional PCET barriers, the inflection zone still exists. And there is only a slight shape change of the Tafel plot at a barrier of 0.6 eV at ca. 1.9 V<sub>SHE</sub>. A high barrier of 1 eV results in the disappearance of the inflection zone as OER will not be able to compete with the Kolbe reaction under these conditions.

Second, in previous studies, the electrode capacitance and potential of zero charge have been found change during Kolbe electrolysis<sup>41,48</sup> and the surface oxidation of the Pt electrode<sup>72</sup>. For simplicity, we had applied constant values of C<sub>H</sub> and U<sub>PZC</sub> in our model.

In **Figure S15**, we evaluated the sensitivity of simulated polarization curve of the Pt(111) $\alpha$ -PtO<sub>2</sub> surface to different values of C<sub>H</sub> and U<sub>PZC</sub>. Similar shapes of polarization curves were obtained, indicating the overall activity trend is largely unaffected by these parameters. However, we noticed that the magnitude of the overall activity is sensitive to C<sub>H</sub> and U<sub>PZC</sub>: Low C<sub>H</sub> and U<sub>PZC</sub> mean larger interfacial fields, which stabilize the Kolbe intermediates further than those for OER. This difference in field-adsorbate stabilization reduces the extent of the inflection zone. **Figure S16** shows the polarization curves computed without field-adsorbate stabilization. The inflection zone is still present, but the onset of Kolbe electrolysis occurs at higher potentials.

### Revisiting previously proposed mechanisms

Based on our simulation results, we revisit the old mechanistic theories proposed in the past century for the Kolbe electrolysis.

Firstly, we find that the coverages of the Kolbe reaction intermediates are not negligible even on the oxidized Pt surface, indicating that Kolbe electrolysis is not a pure solution phase (i.e., homogeneous) reaction, but involves adsorbed species, i.e., CH<sub>3</sub>COO\* and CH<sub>3</sub>\*. This finding makes the free-radical theory<sup>36-38</sup>, and other homogeneous proposals of Kolbe electrolysis, e.g., hydrogen peroxide theory<sup>73</sup> unlikely to be the dominant mechanism, in favor of heterogeneous reaction mechanisms proposed by Conway, Fioshin, and Fleischmann<sup>21</sup>.

Secondly, our model shows that the RDS of OER on Pt oxide surface changes from a OH\* formation (before inflection zone) to H<sub>2</sub>O adsorption (during inflection zone), leading to a passivated OER activity at high potentials, which is further exacerbated by the



existence of Kolbe species. In contrast to the OER model without the Kolbe reaction, OER activity including Kolbe electrolysis is passivated ca.  $0.2 V_{\text{SHE}}$  earlier and lowered by several orders of magnitude. This observation is in agreement with the postulation by Vijn and Conway that OER activity is suppressed at high potentials due to the formation of “barrier-layer” films of Kolbe species<sup>43</sup>.

Finally, our DRC analysis indicates that at high anodic potentials, Kolbe reaction is not determined by the discharge of  $\text{CH}_3\text{COOH}$  on the  $\text{PtO}_2$  surface (cf. Eqn 1), but by the following decarboxylation and dimerization steps. This result refutes the conclusion in Ref<sup>40</sup> that initial discharge of acetate anion is the RDS during the Kolbe electrolysis of acetic acid. Given the uncertainties in DFT calculation, our model shows that both decarboxylation of  $\text{CH}_3\text{COO}^*$  and  $\text{CH}_3^*$  dimerization can determine Kolbe activity on  $\text{PtO}_2$  during the inflection zone. Beyond the inflection zone, Kolbe reaction is mainly determined by the  $\text{CH}_3\text{COO}^*$  decarboxylation. Our simulation results indicate that the RDS for Kolbe reaction does not involve a PCET step, in contrast to previous proposals that directly involve the discharge and deprotonation of acetic acid in the RDS<sup>21</sup>.

## DISCUSSION

To summarize, we presented a detailed mechanistic study of the Kolbe electrolysis of acetic acid on Pt anodes that helps resolve the origin of inflection zone at high overpotentials and the controversy over possible RDS. The field-corrected free energy diagrams indicate that the sluggish deprotonation of  $\text{CH}_3\text{COOH}$  on Pt oxide in aqueous conditions leads to a high overpotential for Kolbe products. The microkinetic simulation shows that the experimentally observed inflection zones (passivated total activity) at high

potentials arise from a shift in RDS of OER from  $\text{*OH}$  formation to  $\text{H}_2\text{O}$  adsorption on oxidized surfaces, which is further exacerbated by the onset of the Kolbe reaction. The RDS for Kolbe reaction during inflection zone is unlikely to be the deprotonation and discharge of acetic acid, but the later chemical steps of  $\text{CH}_3\text{COO}^*$  decarboxylation and/or  $\text{CH}_3^*$  dimerization, which are promoted by adsorbate-field interactions at high potentials. The results presented above suggest that (i) reducing water content in reaction system or using non-oxidative solvents could in principle promote the Kolbe reaction at lower overpotentials; and (ii) finding alternative oxidized surfaces in aqueous conditions with stronger  $\text{CH}_3\text{COO}^*$  binding along with a flexible adsorption configuration and weaker  $\text{H}_2\text{O}^*$  binding relative to Pt anodes could lead to lower overpotentials and higher selectivity towards Kolbe products. Future studies will evaluate new materials for these binding properties.

## EXPERIMENTAL PROCEDURES

### Resource availability

#### *Lead Contact*

Further information and requests for resources should be directed to and will be fulfilled by the lead contact, Karen Chan ([kchan@fysik.dtu.dk](mailto:kchan@fysik.dtu.dk))

#### *Materials Availability*

This study did not generate new unique reagents.

#### *Data and Code Availability*

All the computational data including free energies of reaction species, input files for microkinetic analysis, optimized atomic structures and python scripts for figures are available at [https://github.com/CatTheoryDTU/Kolbe\\_electrolysis\\_mechanisms](https://github.com/CatTheoryDTU/Kolbe_electrolysis_mechanisms).

### **Computational details**

All computational procedures including DFT calculation and microkinetic simulations are provided in the Supplemental Experimental Procedures.

## **ACKNOWLEDGMENTS**

This work was supported by a research grant (29450) from VILLUM FONDEN.

## **AUTHOR CONTRIBUTIONS**

Conceptualization, S.L., N.G., and K.C.; methodology, S.L., N. G., H.P. and K.C.; software, S.L. and H.P.; investigation, S.L., H.P. and N.G.; resources, K.C.; data curation, S.L.; writing – original draft, S.L., H.P. and N.G.; writing – review & editing, S.L., H.P., N.G. and K.C.; visualization, S.L; supervision, K.C. and N.G.; project administration, K.C.; funding acquisition, K.C.

## **DECLARATION OF INTERESTS**

The authors declare no competing interests.

## REFERENCES:

1. Yoshida, J., Kataoka, K., Horcajada, R., and Nagaki, A. (2008). Modern Strategies in Electroorganic Synthesis. *Chem. Rev.* *108*, 2265–2299.
2. Wiebe, A., Gieshoff, T., Möhle, S., Rodrigo, E., Zirbes, M., and Waldvogel, S.R. (2018). Electrifying Organic Synthesis. *Angew. Chem. Int. Ed.* *57*, 5594–5619.
3. Zhu, C., Ang, N.W.J., Meyer, T.H., Qiu, Y., and Ackermann, L. (2021). Organic Electrochemistry: Molecular Syntheses with Potential. *ACS Cent. Sci.* *7*, 415–431.
4. Elsherbini, M., and Wirth, T. (2019). Electroorganic Synthesis under Flow Conditions. *Acc. Chem. Res.* *52*, 3287–3296.
5. Pollok, D., and Waldvogel, S.R. (2020). Electro-organic synthesis – a 21<sup>st</sup> century technique. *Chem. Sci.* *11*, 12386–12400.
6. Wiebe, A., Riehl, B., Lips, S., Franke, R., and Waldvogel, S.R. (2017). Unexpected high robustness of electrochemical cross-coupling for a broad range of current density. *Sci. Adv.* *3*, eaao3920.
7. Chen, Y., Tian, B., Cheng, Z., Li, X., Huang, M., Sun, Y., Liu, S., Cheng, X., Li, S., and Ding, M. (2021). Electro-Descriptors for the Performance Prediction of Electro-Organic Synthesis. *Angew. Chem.* *133*, 4245–4253.
8. Navarro, M. (2017). Recent advances in experimental procedures for electroorganic synthesis. *Current Opinion in Electrochemistry* *2*, 43–52.
9. Rauen, A.L., Weinelt, F., and Waldvogel, S.R. (2020). Sustainable electroorganic synthesis of lignin-derived dicarboxylic acids. *Green Chem.* *22*, 5956–5960.
10. Zhang, P., Sheng, X., Chen, X., Fang, Z., Jiang, J., Wang, M., Li, F., Fan, L., Ren, Y., Zhang, B., et al. (2019). Paired Electrocatalytic Oxygenation and Hydrogenation of Organic Substrates with Water as the Oxygen and Hydrogen Source. *Angew. Chem. Int. Ed.* *58*, 9155–9159.
11. Akhade, S.A., Singh, N., Gutiérrez, O.Y., Lopez-Ruiz, J., Wang, H., Holladay, J.D., Liu, Y., Karkamkar, A., Weber, R.S., Padmaperuma, A.B., et al. (2020). Electrocatalytic Hydrogenation of Biomass-Derived Organics: A Review. *Chem. Rev.* *120*, 11370–11419.
12. Zhao, H., Lu, D., Wang, J., Tu, W., Wu, D., Koh, S.W., Gao, P., Xu, Z.J., Deng, S., Zhou, Y., et al. (2021). Raw biomass electroreforming coupled to green hydrogen generation. *Nat. Commun.* *12*, 1-10.

13. Lucas, F.W.S., Grim, R.G., Tacey, S.A., Downes, C.A., Hasse, J., Roman, A.M., Farberow, C.A., Schaidle, J.A., and Holewinski, A. (2021). Electrochemical Routes for the Valorization of Biomass-Derived Feedstocks: From Chemistry to Application. *ACS Energy Lett.* *6*, 1205-1270.
14. Holzhäuser, F.J., Mensah, J.B., and Palkovits, R. (2020). (Non-)Kolbe electrolysis in biomass valorization – a discussion of potential applications. *Green Chem.* *22*, 286–301.
15. Leech, M.C., and Lam, K. (2020). Electrosynthesis Using Carboxylic Acid Derivatives: New Tricks for Old Reactions. *Acc. Chem. Res.* *53*, 121–134.
16. Schäfer, H.-J. (1990). Recent contributions of kolbe electrolysis to organic synthesis. In *Electrochemistry IV Topics in Current Chemistry.*, E. Steckhan, ed. (Springer-Verlag), 91–151.
17. Ng'ang'a Wanyoike, G., Onomura, O., Maki, T., and Matsumura, Y. (2002). Highly enhanced enantioselectivity in the memory of chirality via acyliminium ions. *Org. Lett.* *4*, 1875–1877.
18. Kurig, N., Meyers, J., Holzhäuser, F.J., Palkovits, S., and Palkovits, R. (2020). (Non-) Kolbe Chemistry Going with the Flow: The Continuous Electrolysis of Biogenic Acids. *ACS Sustainable Chem. Eng.* *9*, 1229–1234.
19. Faraday, M. (1834). Siebente Reihe von Experimental-Untersuchungen über Elektrizität. *Ann. Phys. Chem.* *109*, 433–451.
20. Zersetzung der Valeriansäure durch den elektrischen Strom (1848). *Ann. Chem. Pharm.* *64*, 339–341.
21. Vijh, A.K., and Conway, B.E. (1967). Electrode Kinetic Aspects of the Kolbe Reaction. *Chem. Rev.* *67*, 623–664.
22. Conway, B.E., and Dzieciuch, M. (1963). NEW APPROACHES TO THE STUDY OF ELECTROCHEMICAL DECARBOXYLATION AND THE KOLBE REACTION: PART I. THE MODEL REACTION WITH FORMATE. *Can. J. Chem.* *41*, 21–37.
23. Conway, B.E., and Vijh, A.K. (1967). Energetics and electrode potentials for steps in the kolbe electrosynthesis: A critique. *Electrochim. Acta* *12*, 102–104.
24. Klocke, E., Matzeit, A., Gockeln, M., and Schäfer, H.J. (1993). Electroorganie Synthesis, 55. Influences on the Selectivity of the Kolbe versus the Non-Kolbe Electrolysis in the Anodic Decarboxylation of Carboxylic Acids. *Chem. Ber.* *126*, 1623–1630.
25. Yu, Z., Wang, Y., Cao, X., Li, Y., Ma, T., Zhang, L., Liu, L. and Yue, H., 2021. In-Situ and Real-Time Monitoring of Oxygen Evolution during Kolbe Reaction by Scanning Electrochemical Microscopy. *Int. J. Electrochem. Sci.* *16*, 210240.

26. Nilges, P., dos Santos, T.R., Harnisch, F., and Schröder, U. (2012). Electrochemistry for biofuel generation: Electrochemical conversion of levulinic acid to octane. *Energy Environ. Sci.* *5*, 5231–5235.
27. Qiu, Y., Lopez-Ruiz, J.A., Sanyal, U., Andrews, E., Gutiérrez, O.Y., and Holladay, J.D. (2020). Anodic electrocatalytic conversion of carboxylic acids on thin films of RuO<sub>2</sub>, IrO<sub>2</sub>, and Pt. *Appl. Catal. B: Environ.* *277*, 119277.
28. Yuan, G., Wang, L., Zhang, X., Luque, R., and Wang, Q. (2019). Core–Shell Pt@Ir Nanothorns on Carbon Fiber Paper Electrodes for Carboxylic Acid Valorization via Kolbe Electrolysis. *ACS Sustainable Chem. Eng.* *7*, 18061–18066.
29. Klüh, D., Waldmüller, W., and Gaderer, M. (2021). Kolbe Electrolysis for the Conversion of Carboxylic Acids to Valuable Products—A Process Design Study. *Clean Technol.* *3*, 1–18.
30. Dickinson, T., and Wynne-Jones, W.F.K. (1962). Mechanism of Kolbe’s electrosynthesis. Part 1.—Anode potential phenomena. *Trans. Faraday Soc.* *58*, 382–387.
31. Dickinson, T., and Wynne-Jones, W.F.K. (1962). Mechanism of Kolbe’s electrosynthesis. Part 2.—Charging curve phenomena. *Trans. Faraday Soc.* *58*, 388–399.
32. Dickinson, T., and Wynne-Jones, W.F.K. (1962). Mechanism of Kolbe’s electrosynthesis. Part 3.—Theoretical discussion. *Trans. Faraday Soc.* *58*, 400–404.
33. Gilroy, D., and Conway, B.E. (1965). Kinetic Theory of Inhibition and Passivation in Electrochemical Reactions. *J. Phys. Chem.* *69*, 1259–1267.
34. Bagotzky, V.S., and Vasilyev, Yu.B. (1964). Some characteristics of oxidation reactions of organic compounds on platinum electrodes. *Electrochim. Acta* *9*, 869–882.
35. Fioshin, M.Ya., and Vasil’ev, Yu.B. (1963). Kinetics of anodic and chemical reactions in Kolbe’s electrosynthesis. *Russ. Chem. Bull.* *12*, 393–400.
36. Brown, A.C., and Walker, J. (1891). Elektrolytische Synthese zweibasischer Säuren. *Justus Liebigs Annalen der Chemie* *261*, 107–128.
37. Shukla, S., and Walker, O. (1931). Formation of methane during the electrolysis of potassium acetate, and the mechanism of Kolbe’s electro-synthesis. *Trans. Faraday Soc.* *27*, 35–40.
38. Shukla, S.N., and Walker, O.J. (1932). Anode phenomena in the electrolysis of potassium acetate. Part III. Formation of methane. *Trans. Faraday Soc.* *28*, 457–462.
39. Fleischmann, M., Mansfield, J., and Wynne-Jones, Lord (1965). The anodic oxidation of aqueous solutions of acetate ions at smooth platinum electrodes: part II. The non-steady state of the kolbe synthesis of ethane. *J. Electroanal. Chem.* (1959) *10*, 522–537.

40. Vassiliev, Y.B., and Grinberg, V. (1991). Adsorption kinetics of electrode processes and the mechanism of Kolbe electrosynthesis: Part III. Mechanism of the process. *J. Electroanal. Chem. Interf. Electrochem.* *308*, 1–16.
41. Cerviño, R.M., Triaca, W.E., and Arvía, A.J. (1984). Phenomenology related to the kinetics of Kolbe electrosynthesis. *J. Electroanal. Chem. Interf. Electrochem.* *172*, 255–264.
42. Vasini, E., and Giordano, M. (1989). Voltammetric study of competitive processes and detection of reaction intermediates in the kolbe reaction at Pt electrodes. *Electrochim. acta* *34*, 577–585.
43. Vijh, A., and Conway, B.E. (1967). Potentiostatic and potentiodynamic studies on the kolbe electro-synthesis. *Fresenius' Zeitschrift für analytische Chemie* *230*, 81–95.
44. Conway, B.E., and Dzieciuch, M. (1963). New Approaches to the Study of Electrochemical Decarboxylation and the Kolbe Reaction: Part II. The Model Reaction with Trifluoroacetate and Comparisons with Aqueous Solution Behavior. *Can. J. Chem.* *41*, 38–54.
45. Conway, B.E., and Dzieciuch, M. (1963). NEW APPROACHES TO THE STUDY OF ELECTROCHEMICAL DECARBOXYLATION AND THE KOLBE REACTION: PART III. QUANTITATIVE ANALYSIS OF DECAY AND DISCHARGE TRANSIENTS AND THE ROLE OF ADSORBED INTERMEDIATES. *Can. J. Chem.* *41*, 55–67.
46. Bolzán, A.E., and Arvia, A.J. (1994). Changes in the kinetics of the oxygen evolution reaction induced by oxide films at platinum electrodes. *J. Electroanal. Chem.* *375*, 157–162.
47. Rand, D., and Woods, R. (1972). A study of the dissolution of platinum, palladium, rhodium and gold electrodes in 1 M sulphuric acid by cyclic voltammetry. *J. Electroanal. Chem. Interf. Electrochem.* *35*, 209–218.
48. Conway, B.E., Liu, T.C. (1988). Potential relaxation and interfacial capacitance behaviour of the kolbe coupling reaction at Pt. *J. Electroanal. Chem. Interf. Electrochem.* *242*, 317-322
49. Huang, Y.-F., Kooyman, P.J., and Koper, M.T.M. (2016). Intermediate stages of electrochemical oxidation of single-crystalline platinum revealed by in situ Raman spectroscopy. *Nat. Commun.* *7*, 1-7.
50. Liu, S., Zong, J., Zhao, Z.-J., and Gong, J. (2020). Exploring the initial oxidation of Pt, Pt<sub>3</sub>Ni, Pt<sub>3</sub>Au (111) surfaces: a genetic algorithm based global optimization with density functional theory. *Green Chem. Eng.* *1*, 56–62.
51. Jain, A., Ong, S.P., Hautier, G., Chen, W., Richards, W.D., Dacek, S., Cholia, S., Gunter, D., Skinner, D., Ceder, G., et al. (2013). Commentary: The Materials Project: A materials genome approach to accelerating materials innovation. *APL Materials* *1*, 011002.

52. Nong, H.N., Falling, L.J., Bergmann, A., Klingenhof, M., Tran, H.P., Spöri, C., Mom, R., Timoshenko, J., Zichittella, G., Knop-Gericke, A., et al. (2020). Key role of chemistry versus bias in electrocatalytic oxygen evolution. *Nature* **587**, 408–413.
53. Dickens, C.F., Kirk, C., and Nørskov, J.K. (2019). Insights into the Electrochemical Oxygen Evolution Reaction with ab Initio Calculations and Microkinetic Modeling: Beyond the Limiting Potential Volcano. *J. Phys. Chem. C* **123**, 18960–18977.
54. Kelly, S.R., Kirk, C., Chan, K., and Nørskov, J.K. (2020). Electric Field Effects in Oxygen Reduction Kinetics: Rationalizing pH Dependence at the Pt(111), Au(111), and Au(100) Electrodes. *J. Phys. Chem. C* **124**, 14581–14591.
55. Chen, L.D., Urushihara, M., Chan, K., and Nørskov, J.K. (2016). Electric Field Effects in Electrochemical CO<sub>2</sub> Reduction. *ACS Catal.* **6**, 7133–7139.
56. Vijay, S., Gauthier, J.A., Heenen, H.H., Bukas, V.J., Kristoffersen, H.H., and Chan, K. (2020). Dipole-Field Interactions Determine the CO<sub>2</sub> Reduction Activity of 2D Fe–N–C Single-Atom Catalysts. *ACS Catal.* **10**, 7826–7835.
57. Ringe, S., Morales-Guio, C.G., Chen, L.D., Fields, M., Jaramillo, T.F., Hahn, C., and Chan, K. (2020). Double layer charging driven carbon dioxide adsorption limits the rate of electrochemical carbon dioxide reduction on Gold. *Nat. Commun.* **11**, 1-11.
58. Vijay, S., Ju, W., Brückner, S., Strasser, P., and Chan, K. (2021) Unified Mechanistic Understanding of CO<sub>2</sub> Reduction to CO on Transition Metal and Single Atom Catalysts. *Nat. Catal.* 1-8
59. Weaver, M.J. (1998). Potentials of Zero Charge for Platinum(111)–Aqueous Interfaces: A Combined Assessment from In-Situ and Ultrahigh-Vacuum Measurements. *Langmuir* **14**, 3932–3936.
60. Heinen, M., Jusys, Z., and Behm, R.J. (2010). Ethanol, Acetaldehyde and Acetic Acid Adsorption/Electrooxidation on a Pt Thin Film Electrode under Continuous Electrolyte Flow: An in Situ ATR-FTIRS Flow Cell Study. *J. Phys. Chem. C* **114**, 9850–9864.
61. Fioshin, M.Y., and Vasil'ev, Y.B. (1960). Anode processes in the electrolysis of carboxylic acid salts. In *Doklady Akademii Nauk (Russian Academy of Sciences)*, 879–882.
62. Grabow, L.C., Hvolbæk, B., and Nørskov, J.K. (2010). Understanding Trends in Catalytic Activity: The Effect of Adsorbate–Adsorbate Interactions for CO Oxidation Over Transition Metals. *Top Catal.* **53**, 298–310.
63. Lausche, A.C., Medford, A.J., Khan, T.S., Xu, Y., Bligaard, T., Abild-Pedersen, F., Nørskov, J.K., and Studt, F. (2013). On the effect of coverage-dependent adsorbate–adsorbate interactions for CO methanation on transition metal surfaces. *J. Catal.* **307**, 275–282.



64. Conway, B.E., and Vijn, A.K. (1967). Controlled potential studies on the Kolbe reaction and the role of coadsorbed surface oxides. I. Platinum in trifluoroacetate solutions. *J. Phys. Chem.* **71**, 3637–3654.
65. Ebersson, L., and NILSSON, S. (1968). Studies on the Kolbe Electrolytic Synthesis. *Acta Chem, Scand* **22**.
66. Sato, N., Sekine, T., and Sugino, K. (1968). Anodic Processes of Acetate Ion in Methanol and in Glacial Acetic Acid at Various Anode Materials. *J. Electrochem. Soc.* **115**, 242.
67. Damjanovic, A., and Jovanovic, B. (1976). Anodic Oxide Films as Barriers to Charge Transfer in O<sub>2</sub> Evolution at Pt in Acid Solutions. *J. Electrochem. Soc.* **123**, 374–381.
68. Damjanovic, A., Birss, V.I., and Boudreaux, D.S. (1991). Electron Transfer Through Thin Anodic Oxide Films during the Oxygen Evolution Reactions at Pt Electrodes: I. Acid Solutions. *J. Electrochem. Soc.* **138**, 2549–2555.
69. Birss, V.I., and Damjanovic, A. (1987). Oxygen Evolution at Platinum Electrodes in Alkaline Solutions: I. Dependence on Solution pH and Oxide Film Thickness. *J. Electrochem. Soc.* **134**, 113–117.
70. Suen, N.-T., Hung, S.-F., Quan, Q., Zhang, N., Xu, Y.-J., and Chen, H.M. (2017). Electrocatalysis for the oxygen evolution reaction: recent development and future perspectives. *Chem. Soc. Rev.* **46**, 337–365.
71. Patel, A.M., Vijay, S., Kastlunger, G., Nørskov, J.K., and Chan, K. (2021). Generalizable Trends in Electrochemical Protonation Barriers. *J. Phys. Chem. Lett.* **12**, 5193–5200.
72. Pell, W.G., Zolfaghari, A., and Conway, B.E. (2002). Capacitance of the double-layer at polycrystalline Pt electrodes bearing a surface-oxide film. *J. Electroanal. Chem.* **532**, 13–23.
73. Glasstone, S., and Hickling, A. (1939). The Hydrogen Peroxide Theory of Electrolytic Oxidation. *Chem. Rev.* **25**, 407–441.

**Figure and scheme titles and legends:**

**Scheme 1.** The reaction mechanisms for Kolbe electrolysis.

a) The overall picture for Kolbe electrolysis of carboxylic acids (R-COOH).

The picture includes the Kolbe reactions resulting in the formation of alkanes (highlighted in blue), and the Non-Kolbe reactions resulting in the formation of alkenes, esters and alcohols (Hofer-Moest product).  $R_1$  and  $R_2$  represent disproportionated moieties of the radical  $R^\bullet$ .  $R_3$  represents the  $\beta$ -elimination product of  $R^\bullet$ . For example, if  $R = \text{CH}_3(\text{CH}_2)_n\text{CH}_2$   $n \geq 1$ ,  $R_1 = \text{CH}_3(\text{CH}_2)_n\text{CH}_3$ ,  $R_2 = \text{CH}_3(\text{CH}_2)_{n-1}\text{CH}=\text{CH}_2$ ,  $R_3 = R_2$ . Note that the disproportionation and elimination reactions are not involved in the electrolysis of acetic acid.

b) The Kolbe electrolysis of acetic acid on Pt anodes.

Color coding of atoms: red - oxygen, grey - carbon, white - hydrogen and light grey - platinum.

**Figure 1.** Field effects on reaction intermediates for Kolbe electrolysis and OER.

a) Gibbs free adsorption energy response to field on Pt(111)

b) Gibbs free adsorption energy response to field on Pt(111)@ $\alpha$ -PtO<sub>2</sub> surface

Pt(111):  $C_H = 20 \mu\text{F}/\text{cm}^2$ ,  $U_{\text{PZC}} = 0.3 \text{ V vs SHE}$ ; Pt(111)@ $\alpha$ -PtO<sub>2</sub>:  $C_H = 40 \mu\text{F}/\text{cm}^2$ ,  $U_{\text{PZC}} = 1.5 \text{ V vs SHE}$ . The data points were explicitly calculated with a sawtooth potential and the fitted line was extrapolated from a parabolic fit of these values (details in methods). The dotted lines represent OER intermediates, and the solid lines represent Kolbe reaction intermediates. Parametrized dipole moment ( $\mu$ ) and polarizability ( $\alpha$ ) are shown in the insets. Model slabs are shown with top and side views as insets in a) and b).

**Figure 2.** Free energy diagrams of acetic acid electrooxidation (Kolbe) and OER.

on a) Pt(111) and b) Pt(111)@ $\alpha$ -PtO<sub>2</sub>.  $V_{\text{SHE}} = 1, 2$  and  $2.5$  V at pH = 4.6 and 298 K are applied here to show the potential effect on reaction energetics, with Kolbe reaction in black and OER in red. As for OER, only the thermodynamics of proton-coupled electron transfer steps are considered, which might result in an overestimation of OER activity obtained using microkinetic simulations. This approximation also applies to the deprotonation of CH<sub>3</sub>COOH involved in the Kolbe reaction. c) and d) representative configurations of the initial state (IS), transition state (TS) and final state (FS) obtained using nudged elastic band (NEB) calculations of the C-C bond breaking step of CH<sub>3</sub>COO\* to CH<sub>3</sub>\* and CO<sub>2(g)</sub> on Pt(111) and Pt(111)@ $\alpha$ -PtO<sub>2</sub> respectively.

**Figure 3.** Experimental observations and microkinetic modeling results for Kolbe electrolysis of acetic acid on Pt anodes. a) Experimental polarization curves of Kolbe electrolysis in sodium acetate and acetic acid solutions on a polished Pt anode with different acetic acid concentrations ( $C_a = 0.1, 0.5$  and  $1\text{M}$ ),  $\text{pH} = 4.6$ , at room temperature. The inflection zone is highlighted.<sup>30</sup> b) Simulated polarization curves on  $\text{Pt}(111)@ \alpha\text{-PtO}_2$  surface using  $C_H = 40 \mu\text{F}/\text{cm}^2$ ,  $U_{\text{PZC}} = 1.5 \text{V}_{\text{SHE}}$  c) Simulated partial current density towards OER (dashed lines) and Kolbe reaction on  $\text{Pt}(111)@ \alpha\text{-PtO}_2$  (solid lines) d) Experimental<sup>30</sup> and simulated selectivity of Kolbe reaction vs. OER on Pt anode with  $C_a = 1\text{M}$ ,  $\text{pH} = 4.6$ , at room temperature; e) Simulated coverages of key adsorbates involved in the Kolbe and OER reactions on  $\text{Pt}(111)@ \alpha\text{-PtO}_2$  under the same conditions of d)<sup>30</sup>; f) Degree of rate control (DRC) analysis on  $\text{Pt}(111)@ \alpha\text{-PtO}_2$  (The grey region represents inflection zone). Conditions for microkinetic simulations:  $\text{pH} = 4.6$ ,  $T = 298 \text{K}$ ,  $C_a = 0.001, 0.01, 0.1, 1, 10 \text{M}$ .

**Figure 4.** The experimental (on oxidized Pt anodes) and simulated partial polarization curves on Pt(111) $\alpha$ -PtO<sub>2</sub> of Kolbe electrolysis of acetic acid. Only the first three data points (solid markers) of the experimental Kolbe activity were used for fitting the Tafel slopes due to the potential mass transport limitations of products or other side reactions at higher potentials, while the rest of the data points (hollow markers) were excluded. Experiments by Dickinson and Wynne-Jones: 1M acetic acid, T = 298K, pH = 4.6<sup>30</sup>; Experiments by Cervino et al: 1M acetic acid, T = 303K, pH = 4.9<sup>41</sup>. Conditions for microkinetic simulations: pH = 4.6, T = 298 K, 1M acetic acid.